



Coupling of electrochemical and theoretical techniques to study the interaction of steel / terazole based on 8-hydroxyquinoline in 1.0 M HCl

Z. Rouifi^{1,2}, M. El Faydy², F. Benhiba¹, H. About^{1,2}, H. Ramsis³, M. Boudalia⁴,
H. Oudda¹, R. Touri^{5,6}, M. El M'Rabet⁷, I. Warad⁸, A. Guenbour⁴, B. Lakhrissi²

¹ Laboratory of Separation Processes, Faculty of Science, University IbnTofail, Kenitra, Morocco.

² Laboratory of Agro-Resources, Polymers and Process Engineering, Department of Chemistry, Faculty of Science, Ibn Tofail University, PO Box 133, 14000, Kenitra, Morocco

³ Laboratoire de Spectroscopie, Département de Chimie, Faculté des sciences, Université Ibn Tofail, Kenitra, Morocco

⁴ Laboratory of Electrochemistry, Corrosion and Environment, Faculty of science, Rabat, Morocco.

⁵ Laboratoire d'Ingénierie des Matériaux et d'Environnement : Modélisation et Application, Faculté des Sciences, Université Ibn Tofail, BP 133, Kénitra 14 000, Morocco.

⁶ Centre Régional des Métiers de l'Education et de la Formation (CRMEF), Avenue Allal Al Fassi, Madinat Al Irfane BP 6210 Rabat, Morocco.

⁷ Département DSFA, Unité de chimie, Institut Agronomique et Vétérinaire Hassan II. Rabat, Morocco.

⁸ Department of Chemistry, AN-Najah National University P.O. Box 7, Nablus, Palestine.

Received 21 Apr 2017,
Revised 28 Oct 2017,
Accepted 01 Oct 2017

Keywords

- ✓ 8-Hydroxyquinoline and triazole
- ✓ XC38 steel;
- ✓ electrochemical measurements
- ✓ Theoretical calculation

H. Oudda

ouddahassan@gmail.com
+212698192251

Abstract

A new Heterocyclic organic inhibitor, having a triazole ring, linked with the quinoline ring namely 4-amino-1-((8-hydroxyquinolin-5-yl)methyl)-1,2,3-triazole-5-carbonitrile (AHTC) was prepared and identified by the usual methods as ¹H, ¹³C NMR and Elemental analysis. The influence of AHTC on the protection of XC38 steel against corrosion in 1.0 M HCl solution, have been studied using gravimetric and electrochemical measurement. The obtained results showed that its inhibition efficiency increases with concentration and reaches 90 % at 10⁻³ M. In addition, it is found that the AHTC takes its performance at the temperature range of 298–328 K and its adsorption was well described by the Langmuir isotherm at 298 K. On the other hand, the establishing of correlation between the molecular structures of quantum chemistry indices was carried out using the density functional theory (DFT). Laboratory findings are in concordance with DFT results.

1. Introduction

Corrosion inhibitors have been widely studied in many industries applications to decrease the corrosion rate of materials in contact with aggressive medium [1–17]. These compounds are generally synthetic organic molecules, which contain sulfur, nitrogen, oxygen and/or aromatic rings in their structure. Their inhibition efficiencies mainly depend on their abilities to be adsorbed on metallic surface with the polar groups acting as the reactive centers [18]. In this regards, triazole derivatives of 8-hydroxyquinoline are promising as excellent corrosion inhibitors through their N atoms, π -electron systems and other electronegative atoms. Their uses as essential constituent of many pharmaceutical drugs portray them as potentially non-toxic substances [19,20]. So, several authors have studied the corrosion inhibition of hydroxyquinoline derivatives on mild steel corrosion in acidic medium and they found that these compounds act as excellent inhibitors which their inhibitions increase with their concentrations [21–23].

The objective of the present work is to evaluate the inhibiting properties of new synthesis compound on XC38 steel in 1.0 M hydrochloric acid using classical techniques.

2. Experimental details

2.1. Materials and solutions

The material used is steel whose composition is elucidated in the following table:

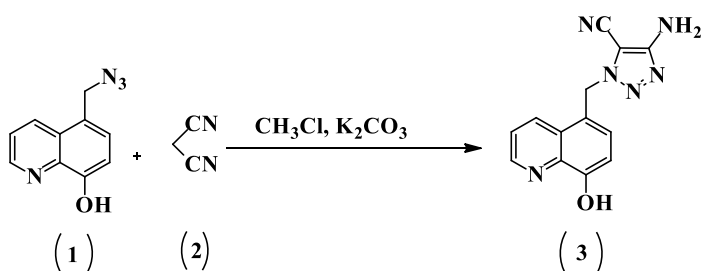
Table 1. Chemical Composition of steel used.

Elements	Fe	C	Cr	P	Si	Mn	Cu	Co	Ni
Wt. %	Balance	0.37	0.077	0.01	0.23	0.68	0.16	0.09	0.059

The electrolyte (1.0 M HCl) was prepared by dilution of an analytical reagent grade 37% HCl with distilled water. On the other hand, the concentration range of AHTC employed was 10^{-6} M to 10^{-3} M, and this range is limited by the solubility of inhibitor.

2.2. Synthesis

The preparation of 4-amino-1-((8-hydroxyquinolin-5-yl)methyl)-1,2,3-triazole-5-carbonitrile (AHTC) is outlined in Scheme 1, starting from 5-azidomethyl-8-hydroxyquinoline (1) which was synthesized according to standard methods described earlier [24], the compound (3) was synthesised by condensation reaction of 2 mol of and malononitrile, 1 mol of 5-azidomethyl-8-hydroxyquinoline (1), 1 mol of triethylamine in chloroform. The resulting mixture was brought to reflux for 24 hours. After completion and cooling to room temperature, water (50 mL) was subsequently added and the product extracted. The combined organic phases were combined, dried over anhydrous sodium sulfate, filtered and evaporated. The obtained residue was purified by column chromatography with hexane/acetone (8:3 to 1:9 v/v) to give compounds 3 (0.83 g, 83 %) as white solid, mp 131-133 °C.



Scheme 1: synthetic route of compounds 3

The compound was identified by

¹H NMR (300 MHz, DMSO-d₆), δppm = 7.115-8.919 (m, 5H, quinoline ring), 4.0242 (s, 2H, quinoline -CH₂-triazole), 9.982 (s, 2H, NH₂).

¹³C NMR (300 MHz, DMSO-d₆), δppm = 42.573 (quinoline-CH₂-), 111.128 - 154.152 (CH, C quinoline and triazole), 16.415 (CN)

Elemental analysis for C₁₃H₁₂N₆O: Calcd: C, 58.20; H, 4.51; N, 31.33%; Found: C, 58.10; H, 4.58; N, 31.40. The ¹H NMR, ¹³C NMR spectra are attached in supplementary data.

2.2. Gravimetric Study

For Gravimetric measurements, the used XC38 steel specimens have a rectangular form of a dimension (1.8cm×1.8cm×0.2cm). Initially, the coupons were treated with different grades of emery paper up 1200 grade, rinsed with distilled water, degreased with acetone and dried at hot temperature, thereafter placing the specimens into the blank solutions for 6 h, and finally the samples were taken out, cleaned with distilled H₂O, dried and weighed. The inhibition efficiency (η_w) was calculated as follows [25]:

$$\eta_w = \frac{\omega_{corr}^0 - \omega_{corr}}{\omega_{corr}^0} \times 100 \quad (1)$$

Where ω_{corr}^0 and ω_{corr} are the corrosion rate values without and with inhibitor, respectively.

2.3. Electrochemical measurements

The electrochemical measurements were carried out using Volta lab (Tacussel- Radiometer PGZ 100) potentiostat and controlled by Tacussel corrosion analysis software model (Voltmaster 4) at under static condition. A saturated calomel electrode (SCE) and platinum electrode were used as reference and auxiliary

electrode, respectively. All potentials given in this study were referred to SCE electrode. While, the working electrode was steel electrode, which immersed in 1M HCl for 30 min to a establish steady state open circuit potential (Ocp). After measuring the Eocp, the electrochemical measurements were performed. The AC-impedance experiments were conducted in the frequency range between 100000 and 0.1 Hz at 0.01 V amplitude. All experiments were carried out under steady conditions (an atmosphere and 298 K). So, the protection efficiencies, η_{EIS} (%), were obtained from the R_{ct} values at different concentrations using the following equation:

$$\eta_{EIS} = \frac{R_{ct} - R_{ct}^0}{R_{ct}} \times 100 \quad (2)$$

Where R_{ct}^0 and R_{ct} are the charge transfer resistance values in the absence and presence of inhibitor, respectively.

Concerning the potentiodynamic polarization, the cathodic Tafel curve was recorded by polarization from Eocp to negative direction while, the anodic Tafel curve was recorded by polarization from Eocp towards positive direction with a scan rate of 0.5 mVs^{-1} and under an atmosphere at 298 K. In addition, the anodic the cathodic Tafel curve was recorded by polarization in this domain under the same conditions already mentioned.

In order to obtain the current densities (i_{corr}), the polarization curves were extrapolated; on the other hand, (i_{corr}) can be find by curve fitting using the equation:

$$i = i_a + i_c = i_{\text{corr}} \left\{ \exp \left[b_a \times (E - E_{\text{corr}}) \right] - \exp \left[b_c \times (E - E_{\text{corr}}) \right] \right\} \quad (3)$$

Where b_a and b_c are the Tafel constants of anodic and cathodic reactions (V^{-1}), respectively. However, b_a and b_c are used to find the Tafel slopes β according to the following formula (4):

$$\beta = \frac{\ln 10}{b} = \frac{2.303}{b} \quad (4)$$

The protection efficiency was estimated from i_{corr} values according to the following equation:

$$\eta_{\text{pp}} = \frac{i_{\text{corr}}^0 - i_{\text{corr}}}{i_{\text{corr}}^0} \times 100 \quad (5)$$

where i_{corr}^0 and i_{corr} are the corrosion current densities for XC38 steel electrode in the uninhibited and inhibited solutions, respectively.

2.4. Computational procedures

All quantum chemical calculations and visualization of the results were performed using "GaussView 5.0.8 software and " and the standard "GAUSSIAN 09 W" program package [26, 27]. The molecular structure of studied compound was optimized using the density functional theory method (DFT/B3LYP) with 6-31 G (d,p) . The quantum chemical parameters such as energy gap ΔE_{GAP} ($E_{\text{HOMO}} - E_{\text{LUMO}}$), global hardness (η), global softness (σ), absolute electronegativity (χ), electrophilicity index (ω) and fraction of transferred electrons (ΔN) which can be calculated using the E_{HOMO} , E_{LUMO} and the following equations [28–32]:

$$\eta = \frac{\Delta E}{2} = \frac{E_{\text{LUMO}} - E_{\text{HOMO}}}{2} \quad (6)$$

$$\sigma = \frac{1}{\eta} = -\frac{2}{E_{\text{HOMO}} - E_{\text{LUMO}}} \quad (7)$$

$$Pi = -E_{\text{HOMO}} \quad (8)$$

$$A = -E_{\text{LUMO}} \quad (9)$$

$$\chi = -Pi \quad (10)$$

The number of transferring electrons (ΔN) was obtained according to the following formula:

$$\Delta N = \frac{\chi_{\text{Fe}} - \chi_{\text{inh}}}{2(\eta_{\text{Fe}} + \eta_{\text{inh}})} \quad (11)$$

Where χ_{Fe} and χ_{inh} describe the absolute electronegativity of Fe and the inhibitory molecule, η_{Fe} and η_{inh} denote respectively the absolute hardness of iron and the inhibitor molecule. Theoretically $\chi_{\text{Fe}} = 7.0 \text{ eV}$ and

$\eta_{\text{Fe}} = 0$ for the calculation of the number of transferring electrons [33].

Using left and right derivatives with respect to the number of electrons, electrophilic and nucleophilic Fukui functions for a site k in a molecule can be defined [34].

$$f_k^+ = P_k(N+1) - P_k(N) \quad (\text{For nucleophilic attack}) \quad (12)$$

$$f_k^- = P_k(N) - P_k(N-1) \quad (\text{For electrophilic attack}) \quad (13)$$

Where, $P_k(N)$, $P_k(N+1)$ and $P_k(N-1)$ are the natural populations for the atom k in the neutral, anionic and cationic species respectively.

3. Results and discussion

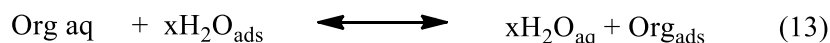
3.1. Weight loss studies

The effect of AHTC on the protection against corrosion of XC38 steel in 1.0 M HCl medium was first evaluated by the weight loss; the obtained results are summarized in Table 2. It is seen that the AHTC inhibits the corrosion of XC38 steel at all concentrations. Indeed, the corrosion rate values decrease with the inhibitor concentration to reach a maximum at 10^{-3} M and the protection efficiency increases to attain 85 %. The best inhibition obtained can be explained by the strong interaction of AHTC at steel surface.

Table 2. Weight loss data of XC38 steel in 1.0 M HCl without and with different concentrations of AHTC at 298 K after 6 h of immersion.

	C_{inh} (M)	W_{corr} ($\text{mg cm}^{-2} \text{h}^{-1}$)	θ	η_w (%)
Blank solution	00	0.4292	-	-
AHTC	10^{-6}	0.1809	0.5785	57
	10^{-5}	0.1356	0.6840	68
	10^{-4}	0.0842	0.8038	80
	10^{-3}	0.0630	0.8532	85

Generally, the corrosion inhibition of steel by heterocyclic organic compounds is demonstrated by the adsorption process. During this process the water molecules adsorbed on the metal surfaces are substituted by the inhibitor molecules according to the following equation. [35, 36]:



Where x present the number of H_2O molecules substituted by one molecule of organic inhibitor.

For the purpose of characterize the adsorption process in corrosion inhibition; there are several models that can be used to describe the adsorption of molecules into solid adsorbent. The most commonly cited models of adsorption isotherms are the Langmuir adsorption isotherm. It is supposed that the AHTC adsorption follows the Langmuir isotherm which the coverage ratio of the metal surface is given by:

$$\theta = \frac{K_{\text{ads}} C_{\text{inh}}}{K_{\text{ads}} C_{\text{inh}} + 1} \quad (14)$$

the latter equation be written differently

$$\frac{C_{\text{inh}}}{\theta} = \frac{1}{K_{\text{ads}}} + C_{\text{inh}} \quad (15)$$

Where θ is the surface coverage and K_{ads} is the adsorption equilibrium constant.

Figure 3 present the variation of C_{inh}/θ by-report C_{inh} . It appears that the slope close to unity and the coefficient correlation ($R^2=1$) equal to unity, this suggests that the Langmuir adsorption model provides the best description of the adsorption behavior.

However, the term K_{ads} values can be estimated from the straight lines C_{inh}/θ axis. This variable is linked to the free energy of adsorption (ΔG_{ads}^*) with the following formula [38, 39]:

$$K_{\text{ads}} = \frac{1}{55.55} \exp\left(\frac{-\Delta G_{\text{ads}}^*}{RT}\right) \quad (16)$$

Where 55.55 value depict the water concentration in solution (mol.L^{-1}), R is the universal gas constant and T is the study temperature.

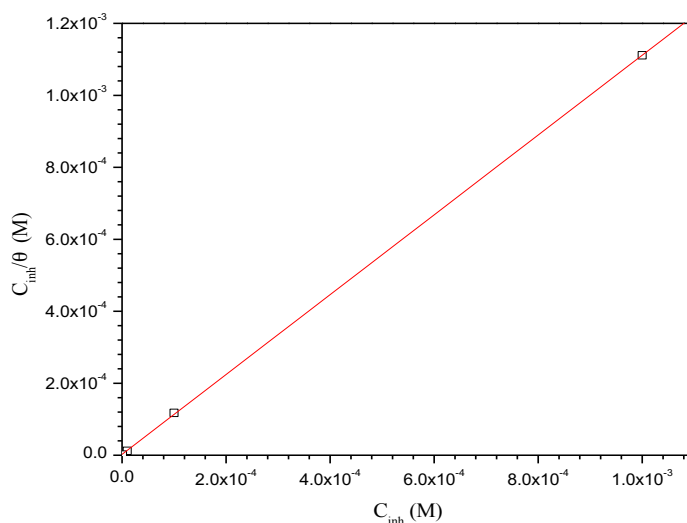


Figure 3: Langmuir adsorption isotherm plot for XC38 steel in 1 M HCl in the presence of the studied AHTC.

The literature review indicates that if the values of the free energy of adsorption in aqueous solution on the order -20 kJ mol^{-1} or less indicate adsorption with electrostatic interaction between the organic molecules and metal surface, while those around or higher than -40 kJ mol^{-1} implies charge sharing between the molecules and the metal [40, 41]. The obtained value is less than -40 kJ mol^{-1} signifies that the adsorption mechanism of the triazole derivative on steel in 1 M HCl solution is typical of chemisorption [42].

3.2. Potentiodynamic polarization curves

The polarization curves for XC38 steel in 1 M HCl at 298K with and without different concentration of triazole derivative are shown in Fig.4. Their extracted kinetics parameters for example: corrosion potential (E_{corr}), cathodic Tafel slopes (β_c) and corrosion current density (i_{corr}) are summarized in Table 3. Moreover, it is obvious that the addition of AHTC cause to strong decrease of current densities for all concentrations. This behavior signifies that the rate of XC38 steel dissolution is decreased in presence of AHTC and justified by the formation of a protective inhibitor film on the metal surface [43, 44].

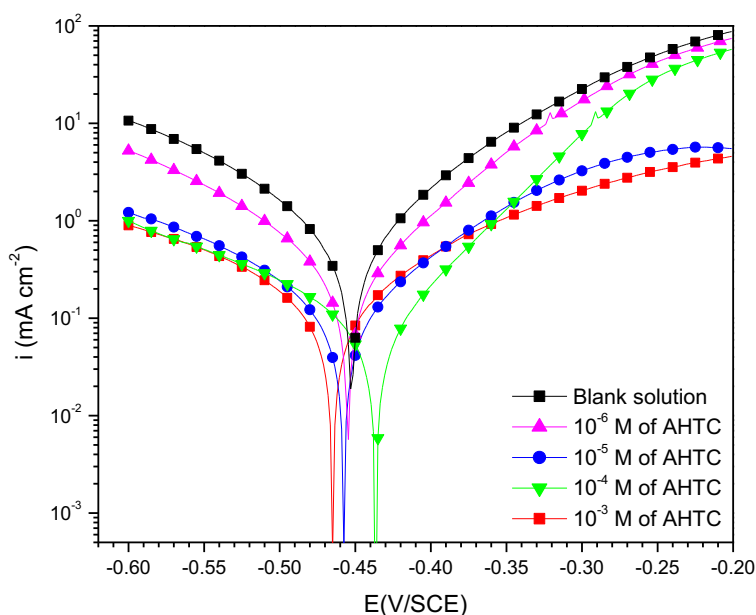


Figure 4: Potentiodynamic polarization curves of XC38 steel in 1.0 M HCl in the absence and the presence of different concentrations of AHTC.

As shown in Figure 4, the AHTC addition lead to reductions of anodic and cathodic currents and a low displacement ($E_{\text{corr}} < 85\text{mV}$) in the corrosion potential (E_{corr}) value, marking that AHTC is a mixed-type inhibitor. However, according to the shape of the polarisation curves, it's clear that this inhibitor has an influence on the cathodic and anodic slopes (β_c and β_a) and neglected the cathodic and anodic processes. This suggests a modification of the mechanism hydrogen evolution reaction of steel [45, 46]. As well, Table 3 indicated that the addition of AHTC favoured a better modification the inhibition efficiency with concentration to reach 90 % at 10^{-3} M, which means that the AHTC has a big affinity to adsorb on the metallic surface.

Table 3. Potentiodynamic parameters of XC38 steel in 1 M HCl containing different concentrations of AHTC.

	C_{inh} (M)	$-E_{\text{corr}}$ (mV/SCE)	i_{corr} ($\mu\text{A cm}^{-2}$)	$-\beta_c$ (mV dec $^{-1}$)	η_{pp} (%)
Blank solution	00	454.4	590.8	101.1	-
AHTC	10^{-6}	457.4	205.2	80.0	65
	10^{-5}	460.1	97.2	124.3	83
	10^{-4}	466.3	85.9	140.1	85
	10^{-3}	439.1	60.7	150.1	90

3.3. Electrochemical impedance spectroscopy

The corrosion behavior of XC38 steel in 1 M HCl in the absence and presence of synthesized compounds is also examined by EIS technique at 298 K. The obtained Nyquist plots are given in Figure 5 and their corresponding parameters are given in Table 4. It is noted that these plots were composed by one depressed semi-circular in the absence and presence of AHTC which is usually assigned to the charge transfer process. All Nyquist curves are simulated an appropriate equivalent circuits given in Fig.6, the circuit used constituted by the electrolyte resistance (R_s), the charge transfer resistance (R_{ct}) and the constant phase element (CPE) represent for the capacitive behavior of the elements adsorbed in the electrical double layer, replaced with capacitance for better fitting.

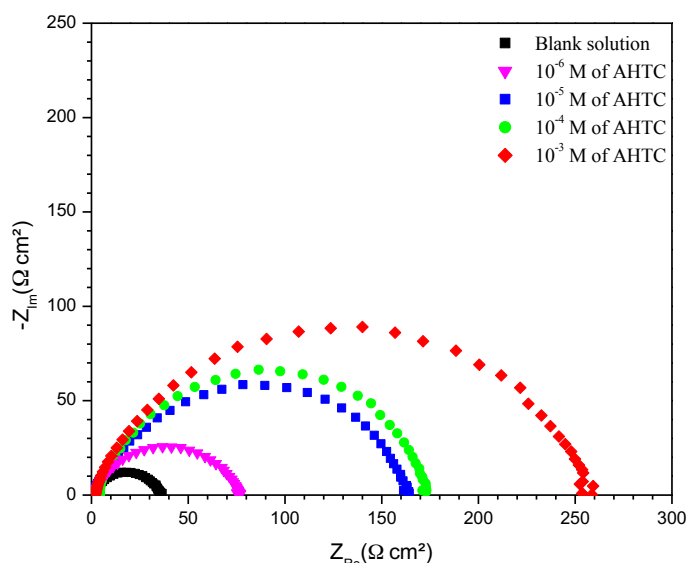


Figure 5: Nyquist plots for XC38 steel at E_{OCP} in 1.0 M HCl in various concentrations of AHTC

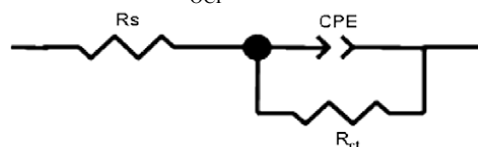


Figure 6: Equivalent circuit applied for EIS analysis.

All impedance parameters are presented in Table 5. It is seen that the values of R_{ct} increase and C_{ct} values decrease with inhibitor concentration. These attributed to the decrease in local dielectric constant and/or increase in thickness of the electrical double layer, indicating that the tested compound works by adsorption at the steel/electrolyte interface [47, 48]. It is obvious that the increase in the inhibitor concentration enhances R_{ct} , and consequently improves the inhibition efficiency to reach its maximum value of 86 % at optimum concentration and this result is in concordance with those obtained by potentiodynamic polarization and gravimetric techniques.

Table 4. Impedance data of XC38 steel in 1 M HCl in the absence and presence of AHTC

	C_{inh} (M)	R_{ct} (Ω cm ²)	C_{dl} (μ F cm ⁻²)	η_{EIS} (%)
Blank solution	00	34.85	114.1	-
	10^{-6}	75.32	84.51	54
AHTC	10^{-5}	165.4	76.22	78
	10^{-4}	170.5	58.97	79
	10^{-3}	258.3	30.8	86

3.4. Effect of temperature

The potentiodynamic polarization curves for XC38 steel in 1M HCl in the absence and presence of 10^{-3} M of AHTC in the temperature range from 298K to 328K are shown in Figures 7 and 8. Their various electrochemical parameters were summarized in Table 5. It can be remarked that the current corrosion density increases with temperature in both inhibited and uninhibited solutions. So, in order to calculate thermodynamic parameters of the corrosion process, Arrhenius Eq. (17) was used :

$$i_{corr} = A \exp\left(-\frac{E_a}{RT}\right) \quad (17)$$

An alternative formulation of Arrhenius equation is:

$$i_{corr} = \frac{RT}{Nh} \exp\left(\frac{\Delta S_a}{R}\right) \exp\left(-\frac{\Delta H_a}{RT}\right) \quad (18)$$

Where A is the Arrhenius pre-exponential factor, E_a the apparent activation energy, R the perfect gas constant, T is the absolute temperature, h plank's constant, N Avogadro's number, ΔS_a the entropy and ΔH_a enthalpy of activation.

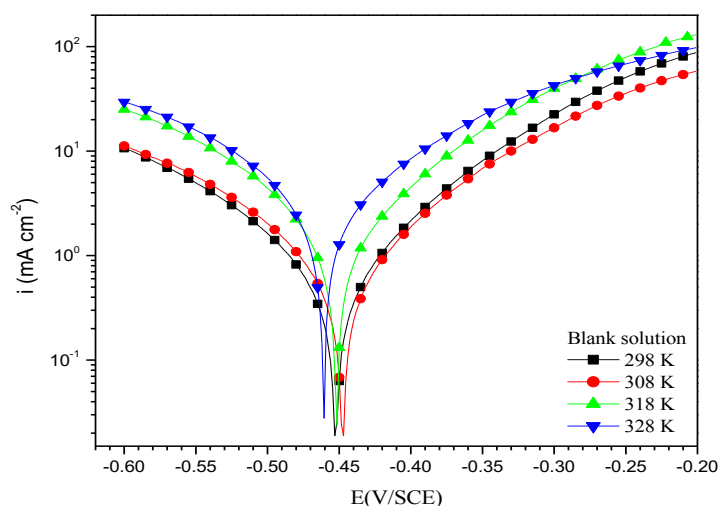
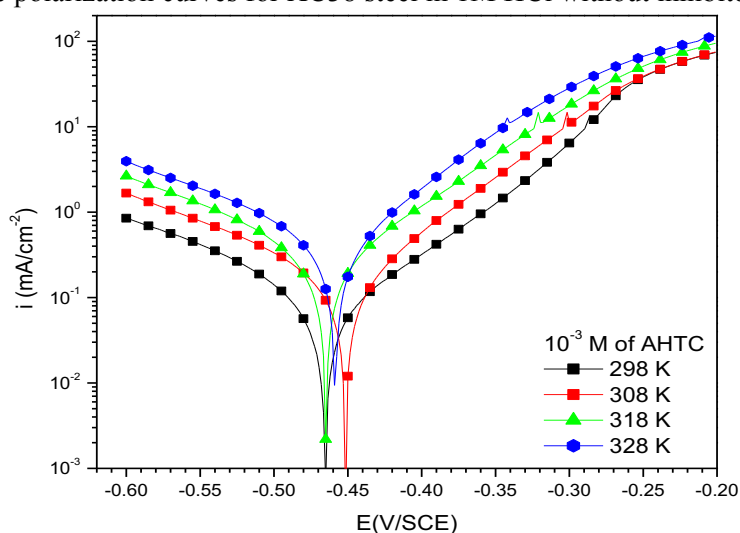
**Figure7:** Potentiodynamic polarization curves for XC38 steel in 1M HCl without inhibitor at different temperatures**Figure 8:** Potentiodynamic polarization curves of XC38 steel in 1.0 M HCl in the presence of 10^{-3} M of AHTC at different temperatures

Table 5. Electrochemical parameters of XC38 steel in 1.0 M HCl in the absence and presence of 10^{-3} M of AHTC at different temperatures.

	T (K)	$-E_{\text{corr}}$ (mV/SCE)	i_{corr} ($\mu\text{A cm}^{-2}$)	$-\beta_c$ (mV dec $^{-1}$)	η_{pp} (%)
Blank solution	298	454.4	590.8	101.1	-
	308	451.1	666.8	104.9	-
	318	454.8	982.4	111.1	-
	328	464.3	2368.5	101	-
10^{-3} M of AHTC	298	67.8	60.7	150.1	90
	308	454.2	134.9	121.2	80
	318	467.4	212.2	102.4	78
	328	462.1	504.6	153.6	78

The E_a was obtained from the slopes of $\text{Ln } i_{\text{corr}}$ versus $(1/T)$ (Figure 9). The straight lines are obtained with a slope $(-\Delta H_a/R)$ and intercept $(\text{Ln } R/Nh + \Delta S_a/R)$ from which these parameters can be extracted (Figure 10).

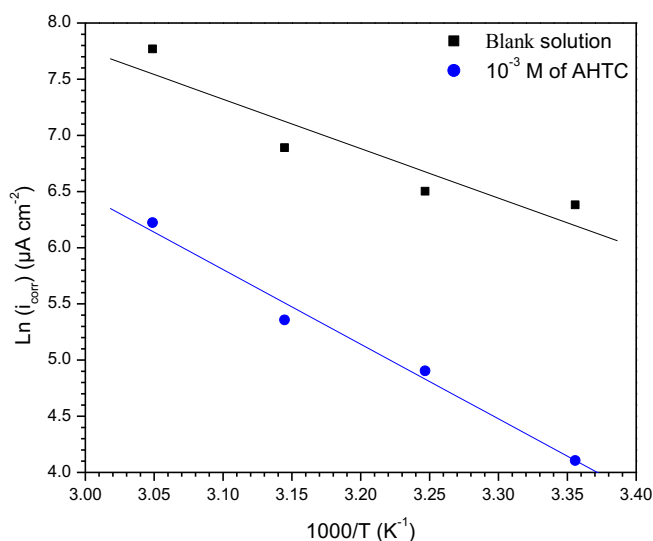


Figure 9: Arrhenius plots for XC38 steel in 1 M HCl in absence and in presence of optimum concentration of AHTC at different temperatures.

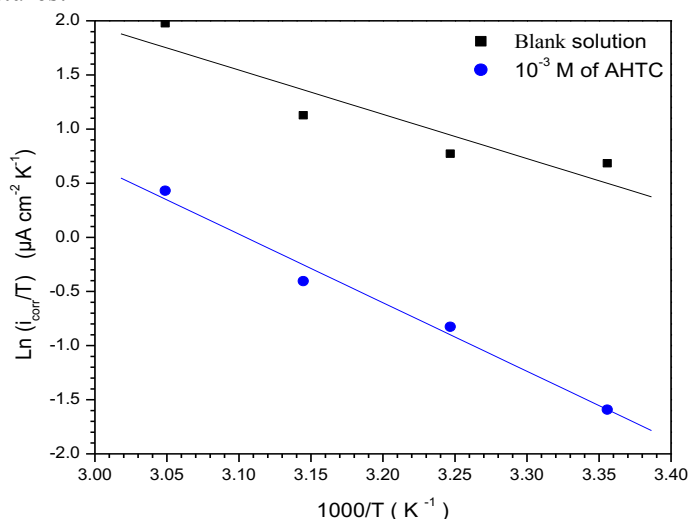


Figure 10: Transition-state plots for XC38 steel in 1 M HCl in absence and presence of optimum concentration of AHTC at different temperatures.

The increase of activation energy E_a value from $36.50 \text{ kJ.mol}^{-1}$ to $55.20 \text{ kJ.mol}^{-1}$ after the addition of the synthesized compound is related to the phenomenon of physisorption of molecules inhibitor on metallic surface [49, 50]. The same observation for ΔH_a values, which increased from $33.98 \text{ kJ.mol}^{-1}$ to $52.64 \text{ kJ mol}^{-1}$ with a positive sign indicating the endothermic nature of dissolution process of steel and the dissolution rate of the latter, is very slow in the presence of tested compound. However, the ΔS_a value increases negatively from -79 J .

$\text{mol}^{-1}.\text{K}^{-1}$ to $-34.08 \text{ J}.\text{mol}^{-1}.\text{K}^{-1}$, this variation interpreted as an ordering and disordering of organic molecules on steel surface [51].

3.5. Quantum chemical calculations

As pointed out in before thinks about, the effectiveness of an inhibitor is identified with the metal-inhibitor communications which depends to the nature and the condition of the metal surface and the chemical structure of the inhibitor. The quantum chemical calculations were employed to give further insight into the mechanism of inhibition action of MHTC. The optimized molecular structure of MHTC are shown in Fig. 11 and a few the quantum compound parameters like as " E_{HOMO} , E_{LUMO} , ΔE , softness (σ), electronegativity (χ), global hardness (ρ), fraction of electron transfer (ΔN) and dipole moment " are posting in Table 6.

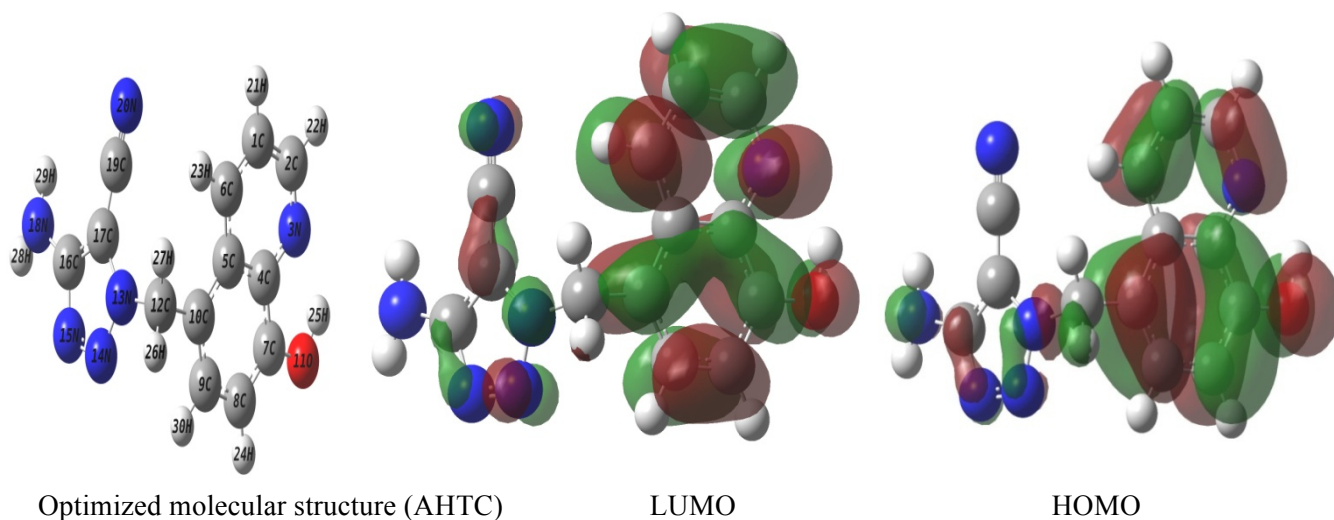


Figure 11: Optimized molecular structures, HOMO and LUMO of AHTC.

The electrostatic potential is viewed as prescient of substance reactivity on the grounds that the negative potential areas are relied upon to be destinations of protonation and nucleophilic assault, while the positive potential locales may demonstrate electrophilic locales. Figure 12 demonstrates the atomic electrostatic potential and the electrostatic capability of the potential Maps. It can be seen that the electrostatic potential around a few gatherings of C-H is sure (blue color) while the electrostatic potential locales around the nitrogen and oxygen molecules are negative (red color). The Mulliken charge distribution with dipole moment vector (a), the contour (b) and the surface representation of the electrostatic potential (c) are given in Figure 12.

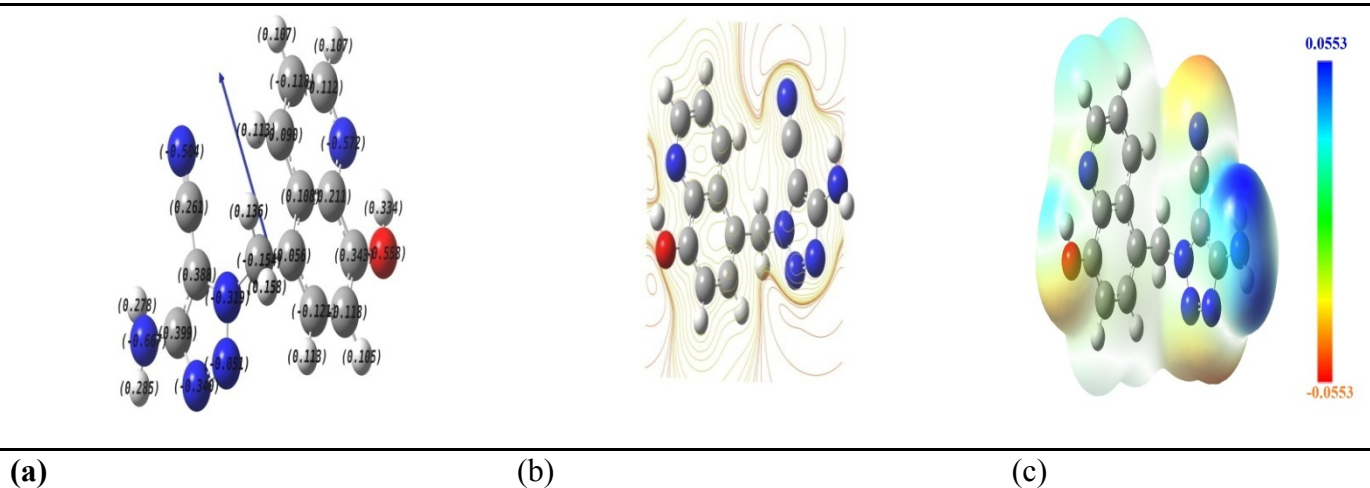


Figure 12: The Mulliken charges with dipole moment and electrostatic properties of AHTC.

According to the molecular orbitals theory of the frontier, the arrangement of a currency state is due to an association between the HOMO and LUMO border orbitals of the reagents High estimation of E_{HOMO} (-5.97 eV) demonstrates the inclination of an atom to give electrons to fitting acceptor particles with low-energy exhaust sub-

atomic orbitals. Expanding estimations of E_{HOMO} facilitate adsorption and therefore enhance the inhibition efficiency by influencing the transport process through the adsorbed layer. The energy of the LUMO demonstrates its capacity to acknowledge electrons [54]. A lower estimation of E_{LUMO} (- 1.739 eV) shows a more prominent likelihood of the particle to acknowledge electrons. Similarly, low estimations of the energy gap ΔE will give great restraint efficiencies, because the excitation energy to remove an electron from the last occupied orbital will be low [55]. However, the χ , η , σ and ΔN esteems are likewise recorded in Table 6.

Table 6. Molecular properties of EHTC obtained from the optimized structure using DFT at the B3LYP/6-31G

Parameters	E_{LUMO} (eV)	E_{HOMO} (eV)	ΔE (eV)	μ (debyes)	η (eV)	σ (eV ⁻¹)	Pi (eV)	χ (eV)	A (eV)	ΔN (eV)	TE (u a)
EHTC	-1.739	-5.972	4.232	1.4124	2.116	0.472	5.972	3.855	1.739	0.743	-905.11

As indicated by a few examinations [56], the parameter of χ is identified with the compound potential, and higher estimation of χ implies better inhibitive execution. Then again, η is equivalent to $\Delta E/2$, and the lower c suggests greater polarizabilities and higher restraint productivity. The parameter of σ is complementary to η ; subsequently high estimation of σ is identified with more proficiency. Estimations of ΔN show inhibitive execution came about because of electrons gifts. In the event that $\Delta N < 3.6$, the hindrance productivity increments with the increments in electron-gift capacity to the metal surface [57]. The Mulliken charge distribution of AHTC is display in Table 7.

Table 7. Fukui function values considering Natural Population analysis (NPA) of AHTC molecule calculated at the B3LYP / 6-31 G (d, p).

Atoms	P(N)	P(N+1)	P(N-1)	f_{K}^+	f_{K}
C1	6.27912	6.23491	6.30910	-0.04421	-0.02998
C 2	5.97327	5.91873	6.01429	-0.05454	-0.04102
N 3	7.46676	7.45399	7.57337	-0.01277	-0.10661
C4	5.87735	5.86051	5.87671	-0.01684	6.4×10^{-4}
C 5	6.07609	6.08784	6.05736	0.01175	0.01873
C 6	6.17706	6.14541	6.27593	-0.03165	-0.09887
C 7	5.64346	5.57623	5.70299	-0.06723	-0.05953
C 8	6.30572	6.22906	6.32037	-0.07666	-0.01465
C 9	6.00613	6.18532	6.24255	0.17919	-0.23642
C 10	6.08053	5.96002	6.13332	-0.12051	-0.05279
O 11	8.68409	8.58563	8.72251	-0.09846	-0.03842
C 12	6.27418	6.29408	6.26609	0.0199	0.00809
N 13	7.20442	7.14578	7.16459	-0.05864	0.03983
N 14	7.09438	7.00049	7.09617	-0.09389	-0.00179
N 15	7.36807	7.25236	7.34985	-0.11571	0.01822
C 16	5.57242	5.64154	5.68068	0.06912	-0.10826
C 17	5.87774	6.02387	6.09936	0.14613	-0.22162
N 18	7.84630	7.76047	7.86601	-0.08583	-0.01971
C 19	5.94417	5.77901	5.76879	-0.16516	0.17538
N 20	7.37263	7.23924	7.38038	-0.13339	-0.00775
H 21	0.74712	0.71965	0.77919	-0.02747	-0.03207
H 22	0.76770	0.73989	0.80591	-0.02781	-0.03821
H 23	0.75975	0.73649	0.77399	-0.02326	-0.01424
H 24	0.69279	0.71117	0.77487	0.01838	-0.08208
H 25	0.48753	0.46334	0.49697	-0.02419	-0.00944
H 26	0.72691	0.69937	0.75394	-0.02754	-0.02703
H 27	0.72691	0.72397	0.75768	-0.00294	-0.03077
H 28	0.55672	0.55220	0.59274	-0.00452	-0.03602
H 29	0.53824	0.56114	0.59424	0.0229	-0.056
H 30	0.87242	0.71828	0.77006	-0.15414	0.10236

The atomic site prone to the nucleophilic attack is related with the greatest estimation of f_K^+ . While the maximum value of f_K^- indicate that this center is preferred for the electrophilic attack [58, 59]. In this examination, it can be found in the Table 6 that the " C (9), C (16) and C (17)" are the most susceptible centers for the nucleophilic attack, and the N (13), C (19) and H (30) are the preferred sites for the electrophilic attack. These atomic sites further strengthening the interaction of the AHTC and the metallic surface.

4. Conclusion

A new ethyl 4-amino-1-((8-hydroxyquinolin-5-yl)methyl)-1H-1,2,3-triazole-5-carbonitrile was synthesis and characterized by ¹H, ¹³C NMR and Elemental analysis. The effect of AHTC on the corrosion inhibition for XC38 steel in 1 M HCl was investigated using experimental and theoretical techniques coupled with Quantum chemical calculations. Overall, there is a great concordance between the gravimetric, electrochemical and theoretical techniques. AHTC compound present a good inhibition performance for XC38 steel in acidic media and its protection efficiency depend upon the concentration and temperature. The data obtained from potentiodynamic polarization data demonstrate that the tested compound acts as mixed type inhibitors. The adsorption of synthesized compound on the XC38 steel follows the Langmuir adsorption isotherm

References

1. A. S. Machin, J. Y. Mann, *Int. J. Fatigue*, 4(4) (1982) 199-208.
2. M. Christov, A. Popova, *Corros. Sci.*, 46(7) (2004) 1613-1620.
3. A. Nagiub, F. Mansfeld, *Corros. Sci.*, 43(11) (2001) 2147-2171.
4. P. C. Okafor, X. Liu, Y. G. Zheng, *Corros. Sci.*, 51(4) (2009) 761-768.
5. M. El Faydy, M. Galai, M. E. Touhami, I. B. Obot, B. Lakhriissi, A. Zarrouk, A. *J. Mol. Liq.* 248 (2017) 1014-1027.
6. A. Ghazoui, R. Saddik, N. Benchat, B. Hammouti, M. Guenbour, A. Zarrouk, M. Ramdani, *Der Pharm. Chem.* 4 (2012) 352.
7. H. Zarrok, R. Saddik, H. Oudda, B. Hammouti, A. El Midaoui, A. Zarrouk, N. Benchat, M. Ebn Touhami, *Der Pharm. Chem.* 3 (2011) 272.
8. A. Zarrouk, B. Hammouti, R. Touzani, S.S. Al-Deyab, M. Zertoubi, A. Dafali, S. Elkadiri, *Int. J. Electrochem. Sci.* 6 (2011) 4939.
9. A. Zarrouk, B. Hammouti, A. Dafali, H. Zarrok, *Der Pharm. Chem.* 3 (2011) 266.
10. A. Ghazoui, A. Zarrouk, N. Bencat, R. Salghi, M. Assouag, M. El Hezzat, A. Guenbour, B. Hammouti, *J. Chem. Pharm. Res.* 6 (2014) 704.
11. H. Zarrok, A. Zarrouk, R. Salghi, H. Oudda, B. Hammouti, M. Assouag, M. Taleb, M. Ebn Touhami, M. Bouachrine, S. Boukhris, *J. Chem. Pharm. Res.* 4 (2012) 5056.
12. H. Zarrok, A. Zarrouk, R. Salghi, M. Assouag, B. Hammouti, H. Oudda, S. Boukhris, S.S. Al Deyab, I. Warad, *Der Pharm. Lett.* 5 (2013) 43
13. M. Belayachi, H. Serrar, H. Zarrok, A. El Assyry, A. Zarrouk, H. Oudda, S. Boukhris, B. Hammouti, E.E. Ebenso, A. Geunbour, *Int. J. Electrochem. Sci.* 10 (2015) 3010.
14. A. Zarrouk, H. Zarrok, R. Salghi, R. Tourir, B. Hammouti, N. Benchat, L.L. Afrine, H. Hannache, M. El Hezzat, M. Bouachrine, *J. Chem. Pharm. Res.* 5 (2013) 1482.
15. H. Zarrok, A. Zarrouk, R. Salghi, M. Ebn Touhami, H. Oudda, B. Hammouti, R. Tourir, F. Bentiss, S.S. Al-Deyab, *Int. J. Electrochem. Sci.* 8 (2013) 6014.
16. D. Ben Hmamou, M.R. Aouad, R. Salghi, A. Zarrouk, M. Assouag, O. Benali, M. Messali, H. Zarrok, B. Hammouti, *J. Chem. Pharm. Res.* 4 (2012) 34984.
17. L. Elkadi, B. Mernari, M. Traisnel, F. Bentiss, M. Lagrenee, *Corros. Sci.*, 42(4) (2000) 703-719.
18. V. Moret, Y. Laras, T. Cresteil, G. Aubert, D. Q. Ping, C. Di, A. Rolland, *Eur. J. Med. Chem.*, 44(2) (2009) 558-567.
19. J. P. Rieu, A. Boucherle, H. Cousse, G. Mouzin, *Tetrahedron*, 42(15) (1986) 4095-4131.
20. G. Achary, H. P. Sachin, Y. A. Naik, T. V. Venkatesha, *Mater. Chem. Phys.*, 107(1) (2008) 44-50.
21. M. El Faydy, M. Galai, R. Tourir, A. El Assyry, M. E. Touhami, B. Benali, A. Zarrouk, *J. Mater. Environ. Sci.* 7 (4) (2016) 1406-1416.
22. H. Lgaz, M. Saadouni, R. Salghi, S. Jodeh, M. Elfaydy, B. Lakhriissi, H. Oudda, *Pharm Lett*, 8 (18): 2016 158-166.
23. B. Himmi, B. Messnaoui, S. Kitane, A. Eddaif, A. Alaoui, A. Bouklouz, M. Soufiaoui, *Hydrometallurgy*, 93(1) (2008) 39-44.

24. A. L. Essaghouani , H. Elmsellem , M. Ellouz , M. El Hafi , M. Boulhaoua , N. K. Sebbar , E. M. Essassi , M. Bouabdellaoui , A. Aouniti and B. Hammouti *Der Pharma Chemica*, 2016, 8(2):297-305
25. Y. Feng, S. Chen, W. Guo, Y. Zhang, G. Liu, *J. Electroanal. Chem.* 602 (2007) 115-122.
26. M. Frisch, G. W. Trucks, H. B. Schlegel, G. E. Scuseria, M. A. Robb, Cheeseman, et al., Gaussian 03, Revision E.01, Gaussian, Inc., Wallingford CT (2004).
27. S. K. Saha, A. Hens, A. RoyChowdhury, A. K. Lohar, N. C. Murmu, P. Banerjee, *Trans*, 2(2014). 489-503.
28. S. K. Saha, P. Ghosh, A. Hens, N. C. Murmu, & P. Banerjee *Physica E Low Dimens Syst Nanostruct*, 66, (2015).332-341.
29. L. Pauling, The nature of the chemical bond and the structure of molecules and crystals: an introduction to modern structural chemistry. Cornell university press (Vol. 18) (1960).
30. R. G. Parr, R. G Pearson, *J. Amer. Chem. Soc*, 105(26) (1983) 7512-7516.
31. P. Geerlings, F. De Proft, W. Langenaeker, Conceptual density functional theory. *Chem. Rev.*, 103(5) (2003)1793-1874.
32. M. M. Kabanda, L. C. Murulana, M. Ozcan, F. Karadag, I. Dehri, I. B. Obot, & E. E. Ebenso, *Int. J. Electrochem. Sci*, 7(2012)5035-5056.
33. S. K. Saha, P. Ghosh, A., Hens, N. C. Murmu, & P. Banerjee, *Physica E Low Dimens Syst Nanostruct* , 66 (2015) 332-341.
34. G. Moretti, F. Guidi, F.n Fabris *Corros. Sci.* 76 (2013) 206.
35. S. Kharchouf, L. Majidi, M. Bouklah, B. Hammouti, A. Bouyanzer, A. Aouniti, *Arab. J. Chem.* 7 (2014) 680.
36. R. Solmaz, *Corros Sci.* 81 (2014) 75.
37. G. Avci, *Colloids Surf's A: Physicochem Eng Asp*, 317(1) (2008) 730-736.
38. F. Xu, J. Duan, S. Zhang, B. Hou, *Mater. Lett*, 62(25) (2008) 4072-4074.
39. F. Bentiss, M. Lebrini, M. Lagrenée, *Corros. Sci.* 47 (2005) 2915.
40. R. Salim, E. Ech Chihbi, H. Oudda, Y. ELAoufir, F. El-Hajjaji, A. Elaattiaoui, A. Oussaid, B. Hammouti, H. Elmsellem and M. Taleb, *Der Pharm. Chem*, 8 (13) (2016) 200.
41. W. Li, Q. He, C. Pei, B. Hou, *Electrochim. Acta*, 52 (2007) 6386-6394.
42. M. V. Fiori-Bimbi, P. E. Alvarez, H. Vaca, C. A. Gervasi, *Corros. Sci*, 92(2015) 192-199.
43. A. Ehsani, M. Nasrollahzadeh, M. G. Mahjani, R. Moshrefi, & H. Mostaanzadeh, *J. Ind Eng Chem*, 20(6) (2014), 4363-4370.
44. M. Mobin, M. Rizvi, *Carbohydr. Polym*, 136 (2016) 384-393.
45. A. Anejjar, R. Salghi, A. Zarrouk, O. Benali, H. Zarrok, B. Hammouti, E. E. Ebenso, *J Assn Arab Univ Basic Appl Sci.ens*, 15(2014) 21-27.
46. O. Benali, L. Larabi, M. Traisnel, L. Gengembre, & Y. Harek, *Appl. Surf. Sci*, 253(14) (2007) 6130-6139.
47. S. K. Shukla, M. A. Quraishi, *Corros. Sci*, 52(2) (2010) 314-321.
48. L. Bammou, M. Belkhaouda, R. Salghi, O. Benali, A. Zarrouk, S. S. Al-Deyab, B. Hammouti, *Int. J. Electrochem. Sci*, 9(2014) 1506-1521.
49. B. Hammouti, A. Zarrouk, S. S. Al-Deyab, I. Warad, *Orient. J. Chem*, 27(2011), 23-31.
50. M. S. Morad, A. K El-Dean, *Corros. Sci* , 48(11) (2006). 3398-3412.
51. T. Laabaissi, H. Lgaz, H. Oudda, F. Benhiba, H. Zarrok, , A. Zarrouk, Touri, *J. Mater. Environ. Sci.* 8 (3) (2017) 1054-1067
52. M. Finšgar, A. Lesar, A. Kokalj, I. Milošev, *Electrochim. Acta*, 53(28) (2008) 8287-8297.
53. D. K. Yadav, B. Maiti, M. A. Quraishi, *Corros. Sci*, 52(11) (2010) 3586-3598.
54. J. Zhang, G. Qiao, S. Hu, Y. Yan, Z. Ren, L. Yu, *Corros. Sci* 53(1), (2011)147-152.
55. N. Khalil, *Electrochim. Acta*, 48(18) (2003) 2635-2640.
56. I. Lukovits, E. Kalman, F. Zucchi, *Corros. Sci*, 57(1) (2001) 3-8.
57. H. Mi, G. Xiao, X. Chen, *Comput. Theor. Chem*, 1072(2015) 7-14.
58. S. K. Saha, P. Ghosh, A. Hens, P. Banerjee,.. *Physica E Low Dimens Syst Nanostruct* , 66(2015) 332-341.

(2018) ; <http://www.jmaterenvirosci.com>